Supporting Information for:

Statistical Thermodynamics for Functionally Rotating Mechanism of the Multidrug Efflux Transporter AcrB

Hirokazu Mishima[1], Hiraku Oshima[2], Satoshi Yasuda[2], and Masahiro Kinoshita*[2]

[1]Graduate School of Energy Science, Kyoto University, Uji, Kyoto 611-0011, Japan
[2]Institute of Advanced Energy, Kyoto University, Uji, Kyoto 611-0011, Japan

**E-mail address:* kinoshit@iae.kyoto-u.ac.jp.

S1. Ununiform Packing of a Protein or Protein Complex

As explained in Figure 2 in the main article, it is desired for a protein or a complex of proteins that the backbones and side chains be closely (efficiently) packed, like a three-dimensional jigsaw puzzle.[1,2] However, this is not always possible, depending on the amino-acid sequence. Even in cases where the overall close packing is not achievable, there are certainly the portions that can closely be packed. It is important to pack such portions preferentially: The other portions cannot participate in the close packing and often become disordered and flexible. For example, the native structure of yeast frataxin[3] has a large valley and a tail. Nevertheless, $|S|$ (S is the solvation entropy) of the native structure is almost minimized[4] because the other portions are closely packed. If an impartial packing was undertaken, the valley and/or the tail could be removed, but the resultant overall packing would become rather loose, causing a larger value of $|S|$.

The preferential packing described above occurs in the case of the AcrB trimer as well. Upon proton binding to one of the three protomers, the structure of this protomer undergoes a significant change with the result that the packing efficiencies of the three protomers become different from one another. Namely, the packing efficiency of the trimer is ununiform. Uniform packing would give rise to lower solvent entropy.

S2. Proton Binding and Dissociation

Let us consider the binding of proton (P) to a protomer (Q) of AcrB, P+Q→PQ.

Denoting the chemical potential of component J (J=P, Q, PQ) by μ_J and setting the activity coefficients at unity yields

$$\mu_P = \mu_{P0} + RT\ln(C_P/C_{P0}),\ \mu_Q = \mu_{Q0} + RT\ln(C_Q/C_{Q0}),\ \mu_{PQ} = \mu_{PQ0} + RT\ln(C_{PQ}/C_{PQ0}) \quad \text{(S1)}$$

where R is the gas constant, T the absolute temperature, C_J (mol/l) the concentration of component J, and the subscript "0" represents the standard state. Setting C_{P0}, C_{Q0}, and C_{PQ0} at 1 mol/l gives

$$\mu_P = \mu_{P0} + RT\ln(C_P),\ \mu_Q = \mu_{Q0} + RT\ln(C_Q),\ \mu_{PQ} = \mu_{PQ0} + RT\ln(C_{PQ}). \quad \text{(S2)}$$

C_P, C_Q, and C_{PQ} are now dimensionless concentrations. The free-energy change upon the binding ΔG is expressed as

$$\Delta G = \mu_{PQ} - \mu_P - \mu_Q = \mu_{PQ0} - \mu_{P0} - \mu_{Q0} + RT\ln\{C_{PQ}/(C_P C_Q)\}. \quad \text{(S3)}$$

Denoting $\mu_{PQ0} - \mu_{P0} - \mu_{Q0}$ by ΔG_0 gives

$$\Delta G = \Delta G_0 + RT\ln\{C_{PQ}/(C_P C_Q)\}. \quad \text{(S4)}$$

ΔG_0 represents the free-energy change upon the production of 1 mol of PQ by the binding of 1 mol of P to 1 mol of Q. ΔG_0 is a negative quantity. When the proton concentration C_P is sufficiently low, $RT\ln\{C_{PQ}/(C_P C_Q)\}$ is positive and large enough to make ΔG positive: Proton dissociation, PQ→P+Q, occurs. Otherwise, ΔG is negative and proton binding, P+Q→PQ, occurs.

Thus, when the proton binding site is exposed to the lower-concentration side, proton dissociation occurs because it also leads to a decrease in the system free energy.

S3. Free-energy Decrease upon Proton Transfer

The free-energy decrease upon the transfer of a single proton from the higher-concentration side to the lower-concentration one can be estimated for the mitochondrial membrane of the liver[5] as follows. It comprises the entropic and energetic components.

We first consider the entropic component. The chemical potentials of proton in the higher-concentration and lower-concentration sides, μ_H and μ_L, are expressed as

$$\mu_H = \mu_{H0} + RT\ln(C_H/C_{H0}),\ \mu_L = \mu_{L0} + RT\ln(C_L/C_{L0}) \quad \text{(S5)}$$

where C_H (mol/l) and C_L (mol/l), respectively, denote proton concentrations in the higher-concentration and lower-concentration sides, and the activity coefficients are set at unity. Setting C_{H0} and C_{L0} at 1 mol/l gives

$$\mu_H = \mu_{H0} + RT\ln(C_H),\ \mu_L = \mu_{L0} + RT\ln(C_L). \quad \text{(S6)}$$

C_H and C_L are now dimensionless concentrations. The free-energy change upon the proton transfer from the higher-concentration side to the lower-concentration one, ΔG, is given by

$$\Delta G = \mu_L - \mu_H = \mu_{L0} - \mu_{H0} + RT\ln(C_L/C_H). \quad \text{(S7)}$$

The use of $\mu_{L0} = \mu_{H0}$ yields

$$\Delta G = RT\ln(C_L/C_H). \quad \text{(S8)}$$

The pH-value in the higher-concentration side is higher than that in the lower-concentration one by 0.75:[5] $\log(C_L/C_H) = -0.75$ and $C_L/C_H = 10^{-0.75}$. Therefore, $\Delta G \sim -1.7RT$. The free-energy decrease upon the transfer of a single proton from the higher-concentration side to the lower-concentration one is $\sim -1.7k_BT$. This comes from the entropic component originating from the entropy of mixing, $\sim 1.7k_B$.

The energetic component can be estimated as follows. The difference between the higher-concentration and lower-concentration sides in the electrostatic potential is 0.168 V.[5] Since the thickness of the membrane is approximately 8 nm,[5] there is the electrostatic-potential gradient (i.e., electric field) of 210,000 V/cm. The energy decrease brought by the transfer of a single proton along the electrostatic-potential gradient is calculated to be $\sim -6.5k_BT$.

The free-energy decrease upon the transfer of a single proton from the higher-concentration side to the lower-concentration one is $\sim -8k_BT$. The free-energy decrease is dependent on the organism, experimental condition, and experimental technique employed. However, the value for the *Escherichia coli* cell is not significantly different: The reported values are around $-6k_BT$.[6] In the main article, we adopt $-8k_BT$ whose entropic and energetic components ($-1.7k_BT$ and $-6.5k_BT$, respectively) are known, and our conclusions are not affected by this adoption at all.

S4. Integral Equation Theory

The integral equation theory (IET) is based on classical statistical mechanics.[7] In this theory, from the system partition function, various correlation functions are defined, and the basic equations satisfied by them are derived. The many-body correlations are also approximately taken into account. As far as the equilibrium properties are concerned, the results obtained are as detailed as those from a computer simulation. In the case of bulk solvent of one component, for example, the temperature, number density, and interaction potential form the input data. By numerically solving the basic equations to obtain the correlation functions, we can calculate the microscopic structure and thermodynamic quantities.

The IET is applicable to analyses on solvation properties of a spherical solute. Thermodynamic quantities of solvation can readily be calculated from the solute-solvent correlation functions obtained via the hypernetted-chain (HNC) closure. A thermodynamic quantity of solvation is the change in the thermodynamic quantity upon solute insertion into the solvent.

When the solvent is water, the water-water and solute-water potentials and correlations are dependent not only on the distance between centers of water molecules but also on the orientation of each water molecule represented by the three Euler angles. Therefore, we use the angle-dependent IET (ADIET).[8-12] In the ADIET the effect of the molecular polarizability is taken into account using the self-consistent mean field (SCMF) theory.[8,9] At the SCMF level the many-body induced interactions are reduced to pairwise additive potentials involving an effective dipole moment. The effective dipole moment thus determined at 298 K and 1 atm is about 1.42 times larger than the *bare* gas-phase dipole moment.

S5. Morphometric Approach

Morphometry is an academic field which treats the shape of a complex object quantitatively. The calculation of S for a large, complex solute molecule like a protein (e.g., a protomer of AcrB) is performed by combining the radial symmetric IET (RSIET) for simple fluids[4] or the ADIET for molecular fluids[8-12] with the morphometric approach (MA).[13,14] The procedure of calculating S of a protein with a prescribed structure comprises the following four steps.

(1) S of a hard-sphere solute with diameter d_U is calculated using the RSIET or ADIET with the HNC closure. The values of S are prepared for sufficiently many different

values of d_U ($0.6 \le d_U/d_S \le 10$). Here, d_S denotes the molecular diameter of the solvent.

(2) The four coefficients are determined by the least square fitting applied to the following equation for hard-sphere solutes (i.e., Eq. (1) in the main article applied to hard-sphere solutes):

$$S/k_B = C_1(4\pi R^3/3) + C_2(4\pi R^2) + C_3(4\pi R) + C_4(4\pi),\ R = (d_U + d_S)/2. \quad \text{(S9)}$$

(3) The four geometric measures of a protein (V_{ex}, A, X, and Y) with a prescribed structure are calculated by means of an extension[14] of Connolly's algorithm.[15,16]

(4) S of a protein with a prescribed structure is obtained from Eq. (1) in the main article where the four coefficients determined in step (2) are used. Smaller $-S$ implies a closer, more efficient packing of the backbone and side chains.

The high reliability of the ADIET-MA hybrid method has been demonstrated for such subjects as the quantitative reproduction of the experimentally measured changes in thermodynamic quantities upon apoplastocyanin folding,[17] elucidation of the mechanisms of cold[4,18] and pressure[19] denaturating of a protein, and proposal of a reliable measure of the thermal stability of a protein.[20]

S6. Tight Packing of Drug-efflux Domains

Overall, the interfaces between portions within the drug-efflux domain are tightly packed. This is because part of each portion is penetrating into the adjacent portion as illustrated in Figure S1.

S7. Calculations Using a Different Structural Data of AcrB

The structural data in "PDB Code: 4dx5"[21] was obtained by X-ray crystallography in which designed ankyrin repeat protein (DARPin) was used for crystallization. The DARPin molecules bind to protomers A and B. Further, a drug molecule (minocycline) binds to protomer B. These molecules are removed from AcrB in the calculations. In this structural model, the number of residues is 1033 for protomers B and E and it is 1044 for protomer A. The 11 residues which are present only in protomer A are removed: Since they are outside the TM domain, the removal is not likely to alter the result of our theoretical calculations. The coordinates of hydrogen atoms cannot be

obtained by the X-ray diffraction. We give hydrogen atoms to the model using the CHARMM biomolecular simulation program[22] through the Multi-scale Modeling Tools in Structural Biology (MMTSB) program.[23] The LJ potential energy for AcrB model is positive and large due to unrealistic overlaps of protein atoms. Such overlaps are removed by the minimization of the energy function using the CHARMM and MMTSB programs. The root mean square deviation (RMSD) for C_α atoms is 0.241 nm between the structures of protomers A and B, 0.324 nm between those of protomers A and E, 0.319 nm between those of protomers B and E.

In what follows, the seven sections in "RESULTS AND DISCUSSION" are copied and pasted with the modifications of the numerical values marked in red. The letters in black do not change at all.

Ununiform Packing Structure of AcrB. Each protomer is considered by decomposing it into three portions, those within the TM, porter, and drug-efflux domains, respectively. Figure S2a–c shows the values of $|S_I{}^M|$ for the three portions of each protomer (the numbers within parentheses) and those *relative to* the smallest value. Within the drug-efflux domain, the differences among the three protomers in the packing efficiency are relatively small. Within the porter domain, protomer B is overall less closely packed than the other two protomers probably due to the presence of an accommodation space for a drug. Within the TM domain, protomer E is overall more closely packed, which is ascribed to proton binding (see "Structural Change of Transmembrane Domain Accompanying Proton Binding").

Here, we comment on the reliability of the difference between $|S_I{}^M|$ and $|S_J{}^M|$ ($I \neq J$). The solvation entropy of a portion is determined primarily by its EV, but most of the EV is taken by the molecular volume of the portion *itself* which has nothing to do with the solvent: The EV is only slightly larger than the molecular volume. Since the molecular volumes of portion M of protomer I and portion M of protomer J share the same value, the solvation entropies of these two portions, which are quite large, are not very different from each other. The difference between the solvation entropies calculated becomes much smaller, but this is because the large contributions to the solvation entropies from the molecular volumes are cancelled out. No serious cancellation of significant digits actually occurs. The EV minus the molecular volume and its contribution to the solvation entropy can accurately be calculated for a given structure of a potion. Thus, the difference between $|S_I{}^M|$ and $|S_J{}^M|$ is much more reliable than one might expect. A similar argument can be made for any of the solvation-entropy changes presented in the later sections.

Figure S2d–g shows the values of $\Delta S_{IJ}{}^M$ and $\Delta S_{IJ}{}^{\mathrm{PD}}$ for the interfaces of two

portions in contact. Overall, the interfaces between portions within the drug-efflux domain are tightly packed. This is because part of each portion is penetrating into the adjacent portion (see Sec. S6 of the Supporting Information). The tight packing through the penetration within the drug-efflux domain makes a substantial contribution to the stability of the trimer. Within each domain, the packing efficiencies of the three interfaces are not significantly different from one another. This is suggestive that impartial, the closest possible packing of all the three interfaces is crucial for the maintenance of high stability of the trimer.

In what follows, we are concerned not with accurate values of $|S_I{}^M|$, $\Delta S_{IJ}{}^M$, and $\Delta S_{IJ}{}^{PD}$ but with their approximate values capturing the physical essence. It is therefore assumed for simplicity that any of the portions within the drug-efflux domain preserves the same structure during each cycle due to the tight packing.

Structural Change of Transmembrane Domain Accompanying Proton Binding. A TM domain comprises the 12 α-helices, TM1–TM12. A proton binds to Asp408 in TM4.[24] For protomers B and E, we calculate the efficiency of the interface packing between each pair of α-helices through the solvent-entropy effect. Slight structural differences are observed between any of the 12 α-helices in protomer B and the same helix in protomer E, but they are taken into account in the calculation. The numerical values given below come primarily from changes in the interface-packing efficiencies, and the contributions from the structural differences mentioned above are much smaller. Since proton binding is present in protomer E while it is absent in protomer B,[24] the change in the efficiency induced by the binding can be estimated. The result is summarized in Figure S3 where $-27k_B$, for example, represents that the solvent-entropy gain originating from the interface packing between TM10 and TM4 becomes lower (i.e., the interface packing becomes less efficient) by $27k_B$ upon the binding. Without the binding, Asp408 in TM4 and Lys940 in TM10 are attracting each other through screened, weak electrostatic interaction. Upon the binding, the negative charge of Asp408 vanishes in essence and the attractive interaction is lost, with the result that the interface between TM4 and TM10 becomes less closely packed. Instead, the interfaces of TM10-TM5, TM10-TM12, TM4-TM2, and TM4-TM3 pairs undergo closer packing properties: The overall packing efficiency becomes higher. Inversely, upon proton dissociation, the opposite changes occur, leading to lower overall packing efficiency. The structural change of the TM domain accompanying proton binding or dissociation becomes a trigger of conformational reorganization of the trimer.

In the trimer, any two of the three TM domains are in contact with each other only through the packing of TM8 and TM1. It has been suggested that the structural modification of TM8 may play significant roles for the drug transport.[24-26] In protomer E, the TM8 helix is extended to the periplasmic side, and the drug entrance is closed.

In protomers A and B, by contrast, the periplasmic extension of TM8 is unwound, and the drug entrance is in the vicinity of the unwound loop and opened. We note that this structural modification of TM8 is taken into account in all of our solvation-entropy calculations through the crystal structure[26] employed. However, we do not know why and how the structural modification occurs. This subject is to be pursued in a future study.

Conformational Reorganization Induced by Proton Binding or Dissociation. The information on the conformational reorganizations caused by proton binding and proton dissociation is included in the conformational transitions (a)→(c) and (c)→(a), respectively, of Figure 4. It is illustrated in Figure S4. In (a), the three protomers share the same structure. The solvation entropy of the trimer in (a) is approximately equal to that in (c). $|S_I{}^M|$ and $\Delta S_{IJ}{}^M$ in (c) are calculated by assuming that the closest possible packing properties are achieved at the three interfaces within the porter and TM domains and they therefore remain unchanged.

The following propositions can then be made:

I. When a proton binds to a protomer, for the portions within the TM domain (see Figure S4a), (i) $|S_I{}^{\mathrm{T}}|$ of this protomer decreases by $130k_{\mathrm{B}}$; (ii) $|S_I{}^{\mathrm{T}}|$ of the protomer next to it in the clockwise direction increases by $80k_{\mathrm{B}}$; and (iii) $|S_I{}^{\mathrm{T}}|$ of the protomer next to it in the counterclockwise direction increases by $50k_{\mathrm{B}}$. The change of (i) is consistent with the increased overall packing efficiency for this protomer within the TM domain described in the last section. For the portions within the porter domain (see Figure S4b), (iv) $|S_I{}^{\mathrm{P}}|$ of this protomer decreases by $70k_{\mathrm{B}}$; (v) $|S_I{}^{\mathrm{P}}|$ of the protomer next to it in the clockwise direction increases by $80k_{\mathrm{B}}$; and (vi) $|S_I{}^{\mathrm{P}}|$ of the protomer next to it in the counterclockwise direction decreases by $10k_{\mathrm{B}}$. The change of (i) also induces an increase in overall packing efficiency for this protomer within the porter domain, giving rise to the change of (iv). The change of (v), which is consistent with the generation of accommodation space for a drug, induces the decrease described in (vi).

II. When a proton dissociates from a protomer, for the portions within the TM domain (see Figure S4a), (vii) $|S_I{}^{\mathrm{T}}|$ of this protomer increases by $130k_{\mathrm{B}}$; (viii) $|S_I{}^{\mathrm{T}}|$ of the protomer next to it in the clockwise direction decreases by $80k_{\mathrm{B}}$; (ix) and $|S_I{}^{\mathrm{T}}|$ of the protomer next to it in the counterclockwise direction decreases by $50k_{\mathrm{B}}$. The change of (vii) is consistent with the decreased overall packing efficiency for this protomer within the TM domain described in the last section. For the portions within the porter domain (see Figure S4b), (vii) $|S_I{}^{\mathrm{P}}|$ of this protomer increases by $70k_{\mathrm{B}}$; (viii) $|S_I{}^{\mathrm{P}}|$ of the protomer next to it in the clockwise direction decreases by

$80k_B$; (ix) and $|S_I^P|$ of the protomer next to it in the counterclockwise direction increases by $10k_B$. The change of (viii) is consistent with the disappearance of accommodation space for a drug.

The physical meaning of these propositions is discussed in the succeeding three sections.

Functional Rotation Induced by Solvent-Entropy Effect. We assume that the proposition made in the last section is always applicable to the conformational reorganization accompanying proton binding or dissociation. The functional rotation can then be interpreted as illustrated in Figure S5. The left, middle, and right conformations in this figure correspond to those of (c), (e), and (g) in Figure 4, respectively. The upper three are within the porter domain and the lower three are within the TM domain. The numbers denote the values of $|S_I{}^M|$ for the three portions of each protomer and those within parentheses denote the changes caused by proton binding (middle) or proton dissociation (right)). An essential point in the functionally rotating mechanism is the following:

"When a proton binds to or dissociates from a protomer, the packing properties of this protomer and its two interfaces are perturbed on the whole in the direction that the solvent entropy is lowered. Hence, the packing properties of the other two protomers are reorganized with the recovery of closely packed interfaces so that the solvent-entropy loss can be compensated and the solvent entropy can be kept almost constant."

Structural Perturbation Caused by Proton Binding. When a proton binds to protomer B as (left)→(middle) in Figure S5, its structure is perturbed in the direction that the solvent entropy is lowered. (The resultant protomer is referred to as protomer B'.) This initially sounds contradictory because $|S_B{}'{}^T|$ and $|S_B{}'{}^P|$ are lower than $|S_B{}^T|$ and $|S_B{}^P|$, respectively (the backbone and side chains of this protomer become more closely packed). It should be noted, however, that the closer packing followed by reduction of the EV gives rise to looser packing of the B-E and B-A interfaces. Within the TM domain, proton binding tries to induce not only the solvent-entropy gain of $130k_B$ arising from the closer packing of protomer B but also the solvent-entropy loss of "$50k_B + 60k_B = 110k_B$" at most caused by the looser packing of the interfaces (see Figure S2(g)). Within the porter domain, proton binding tries to induce the solvent-entropy loss of "$70k_B + 100k_B + 90k_B + 100k_B = 360k_B$" at most originating from the looser packing of the interfaces (see Figure S2(e), (f)) as well as the

solvent-entropy gain of $70k_B$ brought by the closer packing of protomer B. The net gains and losses are $200k_B$ and $470k_B$, respectively. $470k_B$ is the maximum value, but it is probable that the net loss is larger because even slightly looser interface packing causes a significantly large decrease in solvent entropy. Taken together, proton binding to protomer B tries to induce a significantly large loss of solvent entropy. This loss is compensated with the structural reorganization of the other two protomers primarily to recover the close packing of the interfaces.

Structural Perturbation Caused by Proton Dissociation. When a proton dissociates from protomer E' shown in the middle of Figure S5, the structure of this protomer is perturbed in the direction that the solvent entropy is lowered. This can readily be understood because $|S_A{}^T|$ and $|S_A{}^P|$ are higher than $|S_{E'}{}^T|$ and $|S_{E'}{}^P|$, respectively (i.e., the backbone and side chains of this protomer become less closely packed). In this case, the two interfaces are already packed with sufficient tightness and not significantly affected by the proton dissociation. The solvent-entropy loss is compensated with the structural reorganization of the other two protomers which still retains the close packing of the interfaces.

Significance of Trimer Formation. The solvation entropies of protomers A, B, and E are $-36100k_B$, $-36300k_B$, and $-35700k_B$, respectively. An isolated protomer cannot realize the functional structural change "A→B→E→A" by itself. This is because "A→B" and "E→A" would give rise to the solvent-entropy losses of $200k_B$ and $400k_B$, respectively. By forming a trimer, as argued above, the solvent-entropy loss caused by a protomer is always cancelled out by the solvent-entropy gain brought by the other two protomers. It is surprising that as a consequence each protomer accomplishes the functional structural change "A→B→E→A" using the free-energy decrease arising from the transfer of only a single proton, which is as small as $-8k_BT$, with no free-energy barriers. The polyatomic structure of a protomer should possess the feature that the closest overall packing is achievable when three (e.g., neither two nor four) protomers aggregate.

The first recapitulation in "CONCLUSION" is copied and pasted with the modifications of the numerical values marked in red. The letters in black do not change at all.

(1) The functional structural change "A→B→E→A" is essentially infeasible by an isolated protomer. This is because "A→B" and "E→A" would cause the solvent-entropy losses of $200k_B$ and $400k_B$, respectively. By forming a trimer, any solvent-entropy loss caused by a protomer is always cancelled out by the solvent-entropy gain brought by the other two protomers. In the trimer each

protomer is allowed to accomplish the functional structural change.

REFERENCES

(1) Kinoshita, M. Roles of entropic excluded-volume effects in colloidal and biological systems: Analyses using the three-dimensional integral equation theory. *Chem. Eng. Sci.* **2006**, *61*, 2150–2160.

(2) Yasuda, S.; Yoshidome, T.; Oshima, H.; Kodama, R.; Harano, Y.; Kinoshita, M. Effects of side-chain packing on the formation of secondary structures in protein folding. *J. Chem. Phys.* **2010**, *132*, 065105.

(3) Adinolfi, S.; Nair, M.; Politou, A.; Bayer, E.; Martin, S.; Temussi, P.; A. Pastore, A. The factors governing the thermal stability of frataxin orthologues: How to increase a protein's stability. *Biochemistry* **2004**, *43*, 6511–6518.

(4) Oshima, H.; Yoshidome, T.; Amano, K.; Kinoshita, M. A theoretical analysis on characteristics of protein structures induced by cold denaturation. *J. Chem. Phys.* **2009**, *131*, 205102.

(5) Voet, D.; Voet, J. G. *Biochemistry*, 3rd ed.; John Wiley & Sons: New York, 2004.

(6) Kashket, E. R. The proton motive force in bacteria: A critical assessment of methods. *Ann. Rev. Microbiol.* **1985**, *39*, 219–242.

(7) Hansen, J.-P.; McDonald, I. R. *Theory of simple liquids*, 3rd ed.; Academic Press: London, 2006.

(8) Kusalik, P. G.; Patey, G. N. On the molecular theory of aqueous electrolyte solutions. I. The solution of the RHNC approximation for models at finite concentration. *J. Chem. Phys.* **1988**, *88*, 7715–7738.

(9) Kusalik, P. G.; Patey, G. N. The solution of the reference hypernetted-chain approximation for water-like models. *Mol. Phys*. **1988**, *65*, 1105–1119.

(10) Kinoshita, M.; Bérard, D. R. Analysis of the bulk and surface-induced structure of electrolyte solutions using integral equation theories. *J. Comput. Phys.* **1996**, *124*, 230–241.

(11) Cann, N. M.; Patey, G. N. An investigation of the influence of solute size and insertion conditions on solvation thermodynamics. *J. Chem. Phys.* **1997**, *106*, 8165–8195.

(12) Kinoshita, M. Molecular origin of the hydrophobic effect: Analysis using the angle-dependent integral equation theory. *J. Chem. Phys.* **2008**, *128*, 024507.

(13) König, P.-M.; Roth, R.; Mecke, K. R. Morphological thermodynamics of fluids: Shape dependence of free energies. *Phys. Rev. Lett.* **2004**, *93*, 160601.

(14) Roth, R.; Harano, Y.; Kinoshita, M. Morphometric approach to the solvation free energy of complex molecules. *Phys. Rev. Lett.* **2006**, *97*, 078101.

(15) Connolly, M. L. Analytical molecular surface calculation. *J. Appl. Crystallogr.* **1983**, *16*, 548–558.

(16) Connolly, M. L. Computation of molecular volume. *J. Am. Chem. Soc.* **1985**, *107*, 1118–1124.

(17) Yoshidome, T.; Kinoshita, M.; Hirota, S.; Baden, N.; Terazima, M. Thermodynamics of apoplastocyanin folding: Comparison between experimental and theoretical results. *J. Chem. Phys.* **2008**, *128*, 225104.

(18) Yoshidome, T.; Kinoshita, M. Physical origin of hydrophobicity studied in terms of cold denaturation of proteins: comparison between water and simple fluids. *Phys. Chem. Chem. Phys.* **2012**, *14*, 14554–14566.

(19) Harano, Y.; Yoshidome, T.; Kinoshita, M. Molecular mechanism of pressure denaturation of proteins. *J. Chem. Phys.* **2008**, *129*, 145103.

(20) Oda, K.; Kodama, R.; Yoshidome, T.; Yamanaka, M.; Sambongi, Y.; Kinoshita, M. Effects of heme on the thermal stability of mesophilic and thermophilic cytochromes *c*: Comparison between experimental and theoretical results. *J. Chem. Phys.* **2011**, *134*, 025101.

(21) Eicher, T.; Cha, H.-J.; Seeger, M. A.; Brandstätter, L.; El-Delik, J.; Bohnert, J. A.; Kern, W. V.; Verrey, F.; Grütter, M. G.; Diederichs, K.; Pos, K. M. Transport of drugs by the multidrug transporter AcrB involves an access and a deep binding pocket that are separated by a switch-loop. *Proc. Natl. Acad. Sci. U.S.A.* **2012**, *109*, 5687–5692.

(22) Brooks, B. R.; Bruccoleri, R. E.; Olafson, B. D.; States, D. J.; Swaminathan, S.; Karplus, M. CHARMM: A program for macromolecular energy, minimization, and dynamics calculations. *J. Comput. Chem.* **1983**, *4*, 187–217.

(23) Feig, M.; Karanicolas, J.; Brooks, C. L. III MMTSB Tool Set: enhanced sampling and multiscale modeling methods for applications in structural biology. *J. Mol. Graphics Modell.* **2004**, *22*, 377–395.

(24) Yamane, T.; Murakami, S.; Ikeguchi, M. Functional rotation induced by alternating protonation states in the multidrug transporter AcrB: All-atom molecular dynamics simulations. *Biochemistry* **2013**, *52*, 7648–7658.

(25) Murakami, S.; Nakashima, R.; Yamashita, E.; Matsumoto, T.; Yamaguchi, A. Crystal structures of a multidrug transporter reveal a functionally rotating mechanism. *Nature* **2006**, *443*, 173–179.

(26) Seeger, M. A.; Schiefner, A.; Eicher, T.; Verrey, F.; Diederichs, K.; Pos, K. M. Structural asymmetry of AcrB trimer suggests a peristaltic pump mechanism. *Science* **2006**, *313*, 1295–1298.

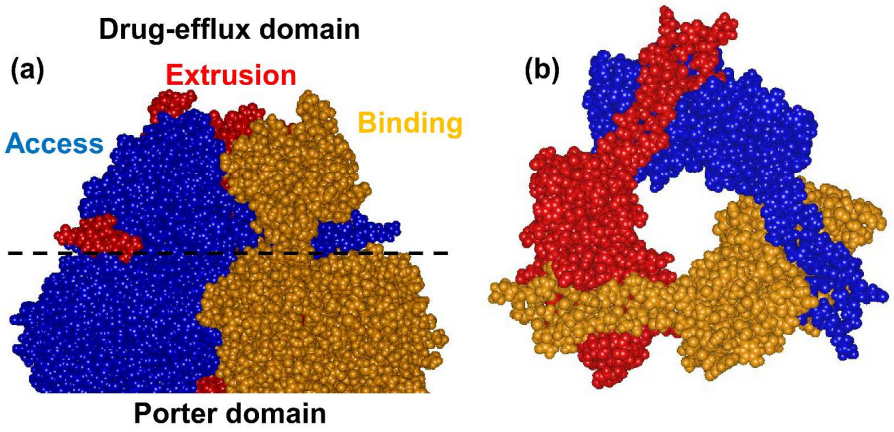

Figure S1. (a) Space-filled representation of drug-efflux (above the broken line) and porter (below the broken line) domains of protomers A (access) and B (binding). (b) Space-filled representation of drug-efflux domain viewed from porter-domain side. This figure is drawn using the DS visualizer 2.5.

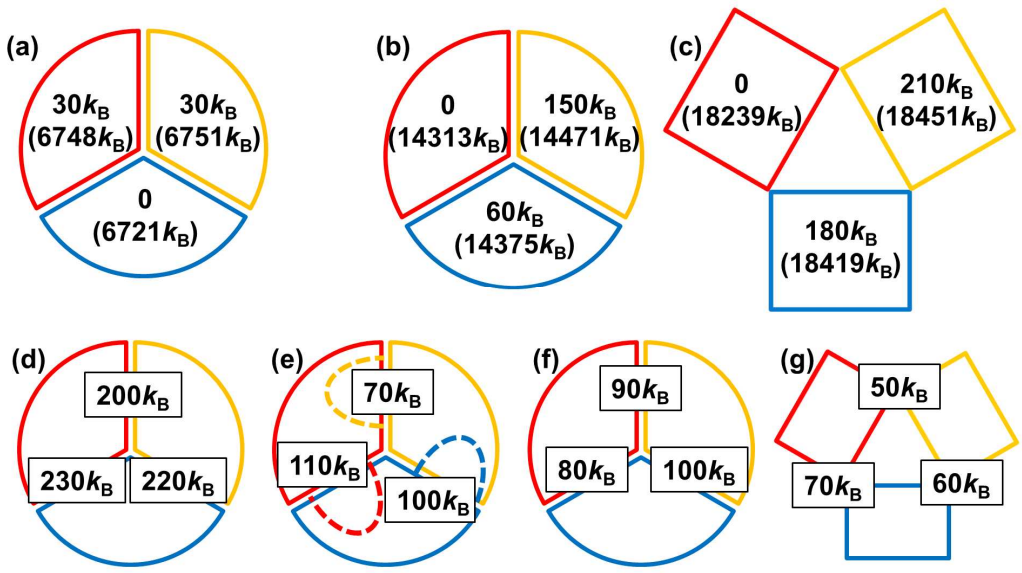

Figure S2. (a)–(c) Values of $|S_I{}^M|$ for the three portions of each protomer (the numbers within parentheses) and those *relative to* the smallest value. The Boltzmann constant is denoted by k_B. Smaller $|S_I{}^M|$ implies that the backbone and side chains of the portion are more efficiently (closely) packed. Conformation 3 shown in Figure 4c is considered. Protomers A, B, and E are drawn in blue, yellow, and red, respectively. A different color represents a different structure. (a) Drug-efflux domain. (b) Porter domain. (c) Transmembrane domain. (d)–(g) Values of $\Delta S_{IJ}{}^M$ and $\Delta S_{IJ}{}^{PD}$ for the interfaces of two portions in contact. They are given within rectangles. Larger $\Delta S_{IJ}{}^M$ or $\Delta S_{IJ}{}^{PD}$ implies that the interface between the two portions is more efficiently packed. Conformation 3 shown in Figure 4c is considered. (d) Interfaces between protomers within drug-efflux domain. (e) Interfaces between protomers within drug-efflux and porter domains, respectively (see Figure S1 in the Supporting Information). (f) Interfaces between protomers within porter domain. (g) Interfaces between protomers within transmembrane domain.

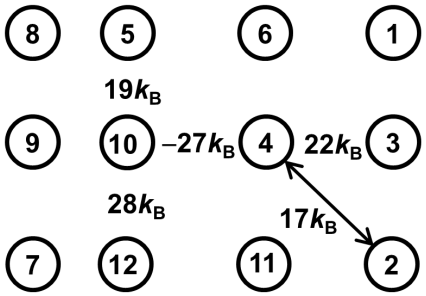

Figure S3. Changes in solvent-entropy gains originating from the interface packing between α-helices within transmembrane domain. The Boltzmann constant is denoted by k_B. The changes are induced by proton binding. "1–12" represent "TM1–TM12", respectively.

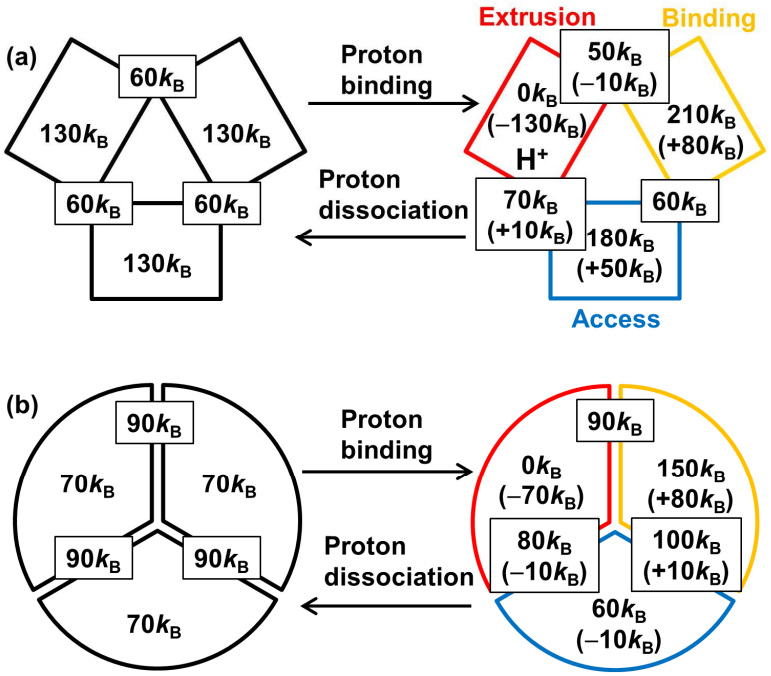

Figure S4. Information on the structural reorganizations caused by proton binding and proton dissociation. The Boltzmann constant is denoted by k_B. Proton binding and proton dissociation correspond to conformational transitions 1→3 and 3→1, respectively (see Figure 4a, c). Relative values of $|S_I{}^M|$ and values of $\Delta S_{IJ}{}^M$ (within rectangles) are given. The numbers within parentheses represent the changes caused by proton binding. Protomers A, B, and E are drawn in blue, yellow, and red, respectively. A different color represents a different structure. (a) Transmembrane domain. (b) Porter domain.

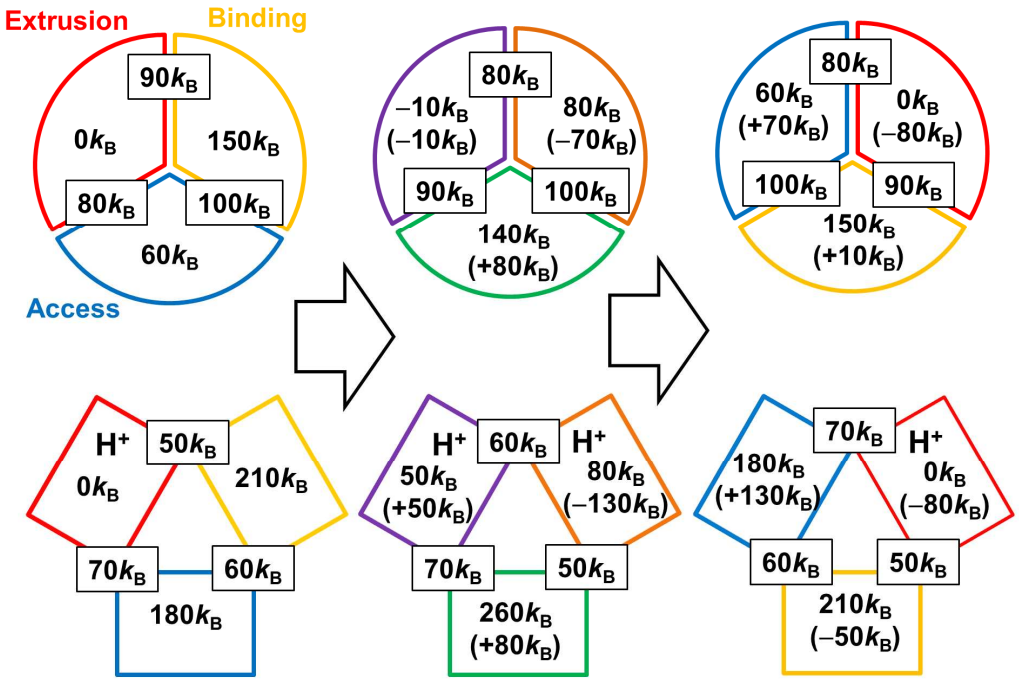

Figure S5. Interpretation of the functional rotation in terms of relative values of $|S_I{}^M|$ and values of $\Delta S_{IJ}{}^M$ (within rectangles). The Boltzmann constant is denoted by k_B. Smaller $|S_I{}^M|$ implies that the backbone and side chains of the portion are more efficiently (closely) packed. Larger $\Delta S_{IJ}{}^M$ implies that the interface between the two portions is more efficiently packed. The numbers within parentheses represent the changes arising from each conformational reorganization of the trimer. The left, middle, and right conformations (they are referred to as (left), (middle), and (right), respectively) correspond to conformations 3, 5, and 7 (see Figure 4c, e, g), respectively. Protomers A, B, E, A', B', and E' are drawn in blue, yellow, red, green, orange, and purple, respectively. A different color represents a different structure. The top is for porter domain. The bottom is for transmembrane domain.